Northumbria Research Link

Northumbria
University
NEWCASTLE

A cohesive network approach for modelling fibre and matrix damage in composite laminates

MW Joosten[a], QD Yang[b], M Blacklock[c] and CH Wang[d]

[a] Deakin University , School of Engineering, Faculty of Science Engineering and Built Environment, 75 Pigdons Road Waurn Ponds, VIC 3217, Australia
[b] Department of Mechanical and Aerospace Engineering, University of Miami, FL 33124, USA
[c] Department of Mechanical and Construction Engineering, Northumbria University, Newcastle upon Tyne, NE1 8ST, United Kingdom
[d] School of Mechanical and Manufacturing Engineering, The University of New South Wales, Sydney, NSW 2052, Australia

Corresponding Author

Dr Mathew W Joosten

Email: mathew.joosten@deakin.edu.au

Address: 75 Pigdons Road Waurn Ponds, VIC 3217, Australia

Abstract: In the current study a high fidelity analysis approach is used to predict failure in notched composite structures. Discrete cracking is explicitly modelled by incorporating cohesive interface elements along potential failure paths. These elements form an interconnected network that allows for interaction between interlaminar and intralaminar failure modes. Finite element models of these configurations were created in the commercial analysis software ABAQUS and a user defined material subroutine (UMAT) was used to describe the behaviour of the cohesive elements. The user material subroutine ensured that the model remained stable despite significant damage, which is a significant challenge for implicit damage simulations. Two analysis approaches were adopted using both the as-measured and in-situ ply strengths. Both approaches were capable of closely predicting the mean ultimate strength for a range of hole diameters, however, the measured ply properties resulted in extensive matrix cracking in the surface ply which resulted in a deviation from the experimentally measured surface strain. The results demonstrate that high fidelity physically based modelling approaches have the ability to compliment experimental programs focussed on the design and certification of composite structures.

(Keywords: Laminates, Strength prediction, Computational modelling, User subroutine (UMAT))

1 Introduction

One of the challenges limiting wide utilisation of fibre reinforced polymeric composites is the difficulty associated with accurately predicting the complex damage progression involving matrix failure and fibre cracking. In the absence of efficient validated analytical or computational models, designers must validate their designs through extensive experimental tests. Experimental validation of a new composite design is both costly and time consuming and, due to the stochastic nature of fibre reinforced composites, it may be difficult to extrapolate a design outside of the empirically derived design envelope.

Strength prediction in notched laminates has been investigated by many researchers. Waddoups et al. [1] used liner elastic fracture mechanics (LEFM) to predict the ultimate strength of notched laminate, however, this approach does not describe the different damage modes that may be present immediately prior to ultimate failure. Whitney and Nuismer [2] recognised that strength predictions based on the stress at the edge of the notch, related to the stress intensity factor, were typically very conservative. To address this limitation they went on to develop the point stress criteria (PSC). The point stress criteria is based on the principal of evaluating the stress away from the edge of the notch. The stress is evaluated at a characteristic distance, however, the characteristic distance can be dependent on both the type and geometry of the notch. While LEFM and the PSC can provide an estimate of the strength of notched laminates, these methods are semi-empirical and do not provide a detailed understanding of the inception and progression of damage. In an effort to understand damage progression in

notched laminates Backlund [3] introduced a damage zone model. The damage zone model (or cohesive zone model) relates material softening to the strain energy release rate to account for the different damage mechanisms. The pioneering work by Backlund paved the way for high fidelity damage models, such as the methodology proposed in the present study.

Presently there are two dominant modelling techniques for simulating the composite failure process, namely, Continuum Damage Mechanics (CDM) and discrete modelling approaches such as the eXtended Finite Element Method (XFEM) and the Augmented Finite Element Method (AFEM). These modelling approaches are significantly different. CDM models simulate failure by altering the elemental stiffness matrix and by doing so smear the damage over the entire element. CDM often incorporates a crack band approach [4]. This approach has shown to provide reasonable prediction of damage initiation and progression in composite structures [5-9], provided the damage laws are adequately calibrated from experimental tests. On the other hand, fracture mechanics approaches, such as the eXtended Finite Element Method (XFEM) and the Augmented Finite Element Method (AFEM), explicitly model the discontinuity of a crack.

Once failure initiates in XFEM and AFEM models additional degrees of freedom are introduced to represent a discontinuity within one element. The discontinuity may have a cohesive traction across the boundary or act as a traction-free crack once full failure has been achieved. A significant advantage of XFEM and AFEM is the ability to simulate arbitrary cracking that is independent of the mesh. The crack does not need to conform

to the element boundaries and may not always remain straight. Crack deflection may occur based on the material, applied loads and redistribution of stresses. Some example of successful applications of XFEM to simulate damage progression in composite structures can be found in Refs. [10-14].

An alternative to both CDM and XFEM, first proposed by Hallett et al. [15], is a hybrid approach where additional degrees of freedom are introduced into a Finite Element (FE) model by inserting three dimensional cohesive elements between three dimensional solid elements. The cohesive elements are inserted along potential crack paths. Damage initiation and propagation is controlled by the cohesive elements and the global behaviour of the model is governed by the continuum elements. The additional degrees of freedom afforded by the cohesive elements allowed discrete cracking to be simulated. This approach is similar to the XFEM, however, the crack path must be specified a priori. Enriching a conventional continuum model with cohesive elements has been adopted by a number of researchers [15-21], however, the published research has focussed on using an explicit integration scheme. In the current study, the authors develop a framework for simulating damage progression in laminated composite structures fabricated from unidirectional plies using an implicit integration scheme.

A composite open hole test specimen is ideally suited to validating damage models as the specimens may exhibit differing failure modes that are dependent on a number of variables which include the material, cure temperature, volume fraction, stacking sequence, block effect, hole diameter, width to diameter ratio (W/D), ply thickness, and

others. It is both expensive and inefficient (and possibly unnecessary) to characterise all of these variables experimentally. High-fidelity simulation techniques [22] that can accurately predict the progressive failure processes, based on a small number of physical experiments that provide key parameter calibration, are in strong demand by the composite community and this is the focus of the present study.

2 Model Description

The present model extends the work of Begley et al. [23] who proposed a brick and mortar model to investigate the behaviour of nacre inspired material topologies. The model consisted of elastic plates (bricks) with elastic-perfectly plastic layers (mortar). Using the brick and mortar approach allows the mortar to be assigned a material property that is independent of the orientation of the joints, either horizontal or vertical. Applying this approach to a unidirectional composite material requires a number of unique material properties that are dependent on the orientation and location of the mortar layers. The present approach facilitates discrete cracking of unidirectional composites by adopting a hybrid analysis approach employing both solid and cohesive elements to represent the bricks and mortar respectively. The solid elements are assigned linear-elastic material properties and bi-linear failure laws applied to the cohesive elements. The present model allows for three possible failure modes:

- Intralaminar matrix failure (matrix splitting)
- Intralaminar fibre rupture
- Interlaminar matrix failure (delamination)

The three failure modes require unique failure laws, see the follow Sections for further details. A two ply [0,90] laminate, schematic representation shown in Figure 1, can be used to illustrate the numerical framework before applying the methodology to a generic laminate. Four solid elements are used to represent the unidirectional plies. Cohesive elements are inserted between ply boundaries. Unique failure laws are applied to the cohesive elements to represent the three possible failure modes. The vertical elements simulate either fibre failure or intralaminar matrix failure depending on the ply orientation. The horizontal elements that are inserted between plies of differing orientations simulate interlaminar failure.

Please insert figure here.

Figure 1: Schematic representation of a brick and mortar modelling approach applied to a unidirectional fibre reinforced composite. Note: the deformed configuration shows an exaggerated displacement.

To extend the modelling approach into three-dimensions an example of a generic three ply unidirectional laminate is shown in Figure 2. Cohesive elements used to represent intralaminar matrix cracking (bold red lines) are inserted parallel to the fibre direction. Additional cohesive elements are inserted orthogonally to the fibre direction to represent fibre rupture (bold blue lines). Cohesive elements are inserted between plies of differing orientations (bold magenta lines). The cohesive elements form an integrated network that allows failure of the specimen to be simulated. Discrete representation of matrix and fibre failure allows for interaction between the three possible failure modes. Final failure of the structure is achieved once the cohesive network forms a continuous failure path through the thickness of the laminate.

Please insert figure here.

Figure 2: Representation of a [0,45,90] laminate modelled with an integrated cohesive network. The filled yellow circles represent nodes and the bold blue, red and magenta lines represent cohesive elements inserted to represent fibre failure, intralaminar matrix failure and interlaminar matrix failure respectively. Note: The lower corner of the 0° ply has been removed to facilitate visualisation of the cohesive network.

All cohesive elements are governed by the same element formulations, however, implementation of the three possible failure modes require different failure laws. In order to describe the modelling approach an overview of the cohesive damage model will be presented first. The specific formulations governing the three possible failure modes will then be described.

2.1 Three-dimensional cohesive model

The model to describe matrix failure (interlaminar and intralaminar) is based on the work of Turon et al. [24] and the model is available in the ABAQUS element library. In the current study he model described in Ref. [24] was implemented in ABAQUS standard using a user defined material subroutine (UMAT). The benefit of implementing the model as a user defined material subroutine is the ability to include differing material behaviours to represent the three possible failure modes. The material models can be used with all of the cohesive elements available within the ABAQUS element library. The formulation of the material model representing fibre failure is different to the matrix failure modes and will be described separately. The traction stress vector, $\boldsymbol{t}$, consists of three components, normal, longitudinal shear and transverse shear. Subsequent mathematical notation will denote these components using the subscripts n, s and t. When the material subroutine is called the current strain and current strain increment

are provided. These strains can be converted to equivalent displacements by multiplying by the effective element thickness, T. If the effective element thickness is set to unity the strain is equal to the displacement at the integration point. The effective element thickness is typically set to unity when the physical element thickness is zero. The nominal elemental displacements, δ_i, are given by:

$$\delta_i = T\varepsilon_i \tag{1}$$

where $i=n,s,t$.

The behaviour of the element can then be written as:

$$\boldsymbol{t} = \begin{bmatrix} \sigma_n \\ \tau_s \\ \tau_t \end{bmatrix} = \boldsymbol{K\varepsilon} = \begin{bmatrix} t_n & 0 & 0 \\ 0 & t_s & 0 \\ 0 & 0 & t_t \end{bmatrix} \begin{bmatrix} \varepsilon_n \\ \varepsilon_s \\ \varepsilon_t \end{bmatrix} \tag{2}$$

It should be noted that there is no coupling between modes as the off axis terms in the stiffness matrix are zero.

The damage variable, *D*, represents degradation of the material and is related to the amount of dissipated energy. When *D* is equal to zero, no energy has been dissipated and the response is purely elastic and when *D* is equal to unity the material is fully damaged and the traction vector is fully degraded. The generalised form of the damage function is given by:

$$D = \frac{\delta^u(\delta - \delta^0)}{\delta(\delta^u - \delta^0)} \tag{3}$$

where δ is an equivalent displacement and δ^0 and δ^u are the displacements that correspond to damage onset and ultimate failure respectively. The stress components

of the traction separation model are related to the damage function by the following relations:

$$t_n = \begin{cases} (1-D)t_n^0 & if \quad \varepsilon_n > 0. \\ t_n^0 \end{cases} \tag{4}$$

where the superscript ^{0} represents the initial un-damaged stiffness. In the current formulation of the model, it is assumed that the shear stiffness is identical in the longitudinal and transverse directions:

$$t_s = t_t = (1-D)t_s^0 \tag{5}$$

A 'zig zag' traction separation law is used to improve the stability of models with multiple interacting failure paths and elements with significant damage [5, 25]. This law alleviates convergence difficulty by introducing piecewise constant positive stiffness in each load increment. Detailed formulations of the zig zag softening law can be found in [6, 26]. The specific model formulations describing matrix cracking and fibre rupture will be described in the following Sections.

2.2 Modelling Intralaminar Failure

A unidirectional ply typically exhibits two failure modes, namely, matrix failure and fibre failure as shown in Figure 3. The present model can represent both of these failure modes by inserting cohesive elements along potential failure paths. The implementation of these failure modes will be described in the following sections.

Please insert figure here.

Figure 3: Intralaminar failure modes (left) fibre failure (right) matrix failure.

2.2.1 Matrix Cracking

Matrix failure is represented by three-dimensional cohesive elements inserted between three-dimensional continuum elements. The cohesive elements are oriented such that the coordinates n, s and t in the elemental coordinate system correspond to 22, 12 and 23 in the ply coordinate system. Under pure mode loading, the onset of failure, or failure initiation, occurs when the traction stress exceeds the material strength related to the mode of failure, either normal or shear. To account for failure onset under mixed mode loading conditions a quadratic stress based onset criteria is introduced:

$$\left(\frac{\langle\sigma_{22}\rangle}{S_{22}}\right)^2 + \left(\frac{\tau_{12}}{S_{12}}\right)^2 + \left(\frac{\tau_{23}}{S_{23}}\right)^2 \leq 1.0 \quad (6)$$

Where σ_{22}, τ_{12} and τ_{23} are the cohesive stresses expressed in the local coordinates as shown in Figure 2. S_{22}, S_{12} and S_{23} are the transverse tensile strength, in-plane shear strength, and out-of-plane shear strength, respectively. The B-K law [27] was used to represent energy dissipation under a generalised loading condition:

$$G_C = G_I + (G_{II} - G_I)B^{\eta} \quad (7)$$

where G_C is the critical strain energy release rate, G_I and G_{II} are the mode I and mode II strain energy release rates respectively. In the present model it is assumed that the critical strain energy release rates in the longitudinal and transverse shear directions are equal. B is a measure of mode mixity and η is used as a fitting parameter.

2.2.2 Fibre Failure

Fibre failure is represented by three-dimensional cohesive elements inserted between three-dimensional continuum elements. The cohesive elements are oriented such that the coordinates n, s and t correspond to 11, 12 and 23 in the ply coordinate system. A stress based criteria is used to define the onset of fibre failure:

$$\frac{<\sigma_{11}>}{S_{11}} = 1 \tag{8}$$

Where σ_{11} is the stress in the fibre direction and S_{11} is the mean ultimate fibre strength. Damage evolution is governed by normal displacement in the fibre direction, δ_{11}, and is similar to the strain based damage evolution typically used to model fibre rupture using a continuum damage mechanics approach. The nominal form of the fibre damage variable, D_f, is a function of the normal tractions and is determined using the following expression:

$$D_f = \frac{\delta_{11}^u(\delta_{11} - \delta_{11}^0)}{\delta_{11}(\delta_{11}^u - \delta_{11}^0)} \tag{9}$$

Where δ_{11} is the elemental displacement in the fibre direction and δ_{11}^0 and δ_{11}^u are the displacements that correspond to damage initiation and ultimate failure respectively. The onset and ultimate displacements are calculated using the following expressions:

$$\delta_{11}^0 = \frac{S_{11}}{t_n} \tag{10}$$

and

$$\delta_{11}^{u} = \frac{2G_{ft}}{S_{11}} \tag{11}$$

where t_n is the traction of the cohesive element in the fibre direction (typically greater than 10^7 N/mm) and G_{ft} is the critical strain energy release rate associated with fibre rupture.

Again, the stability of the model was improved using a zig-zag softening law. In the current study, the fibre damage is only dependent on the axial traction, however, the shear tractions in the cohesive formulation are degraded based on the fibre damage function. Damaging these components will ensure that the cohesive element does not provide any traction when the damage function is equal to unity and behaves like a discrete failure. This type of approach has been used to represent fibre failure in three-dimensional CDM models for unidirectional fibre reinforced composites [7, 9].

Fibre failure due to compressive damage has not been incorporated into the material models used in this study. The current model focusses on evaluating fibre reinforced composite structures under tensile loading conditions. Within the framework of the current model, compressive fibre damage could be incorporated within the continuum elements and this would require no modification to the existing cohesive failure models, however, this is outside the scope of the current study and was not implemented in the present model.

2.3 Modelling Interlaminar Failure

Interlaminar matrix failure or delamination is represented by three-dimensional cohesive elements inserted between plies of differing orientations. The cohesive elements are oriented such that the coordinates n, s and t correspond to 33, 13 and 23 in the ply coordinate system. The implementation of the damage model is similar to the interlaminar damage model described in Section 2.2.1. To account for failure onset under mixed mode loading conditions a quadratic stress based onset criteria is introduced:

$$\left(\frac{\langle\sigma_{33}\rangle}{S_{33}}\right)^2 + \left(\frac{\tau_{13}}{S_{13}}\right)^2 + \left(\frac{\tau_{23}}{S_{23}}\right)^2 \leq 1.0 \qquad (12)$$

where σ_{33}, τ_{13} and τ_{23} are the cohesive stresses and S_{33}, S_{13} and S_{23} are the mean ultimate static strengths. The B-K law [27] was used to represent energy dissipation under a generalized loading condition:

$$G_C{}^i = G_I{}^i + \left(G_{II}{}^i - G_I{}^i\right)B^\eta \qquad (13)$$

where the superscript i indicates that the energy release rates represent interlaminar failure. In the present model it is assumed that the critical strain energy release rates in the longitudinal and transverse shear directions are equal, hence the mode II critical strain energy release rate, $G_{II}{}^i$, is used to represent shear driven crack propagation. The critical mode II and mode III strain energy release rates, $G_{II}{}^i$ and $G_{III}{}^i$ are not necessarily equal and it has been shown that the mode III strain energy release rate is typically larger than the equivalent value for mode II [28]. Therefore using the mode II strain energy release rate to simulate shear driven crack propagation is a conservative assumption

and this material property can be measured using ASTM D7905 [3]. As with the intralaminar failure model a zig-zag softening law was used to improve the stability of the model.

3 Numerical Modelling Approach

This section presents numerical simulations of OHT tests of CFRP laminates with various hole diameters to verify and validate the proposed methodology. Experimental results [29] demonstrate a sensitivity to the size of the hole when the W/D ratio remains constant. The ability of the modelling methodology to predict this trend will be examined and the results presented in the following section. The laminate material is IM7/8552, and its properties are listed in Table 1 & Table 2. It should be noted that the critical strain energy release rates for intralaminar and interlaminar were assumed to be identical. It has been demonstrated by Czabaj and Ratcliffe [30] that for IM7/8552 the initiation fracture toughness in mode I is independent of the orientation of the fracture plane. In the present study it is therefore assumed that the mode II critical strain energy release rate is also independent of the orientation of the fracture plane. To account for residual thermal stresses that occur during manufacturing, an initial analysis step was performed where the model was cooled from the cure temperature to room temperature. The resulting temperature differential was -160°C.

Please insert table here.

Table 1: Orthotropic Material Properties for IM7/8552

Please insert table here.

Table 2: Strength and Fracture Energies Associated with Fibre Rupture and Matrix Cracking (IM7/8552)

3.1 Generating a FE Model with an integrated cohesive network

Several researchers have simulated discrete cracking in composite structures using cohesive elements [15-21]. Two alternate approaches have been proposed by Hallett et al. [15] and Bouvet et al. [17]. Hallet et al. [15] simulated intralaminar matrix cracking by introducing cohesive failure paths tangential to the edge of an open hole. The strip of cohesive elements was aligned with the fibre direction of each ply. Experimental observations demonstrated that intralaminar matrix splitting occurred tangential to the open hole and therefore two cohesive strips were only inserted on either edge of the hole. As an explicit solver was used, small degenerated elements adjacent to the hole were removed to ensure that these elements did not adversely affect the numerical timestep. Removal of these degenerated elements resulted in an oval shaped hole with flat sides in the FE model. The geometry of the final FE model was different to the experimental coupon, however, the numerical failure mode was similar to experimental observations. It is unclear if the mismatch in geometry between the experimental coupon and numerical model influenced the results. Bouvet et al. [17] adopted a different approach where elements were selectively deleted around the notch creating a discretised stepped discontinuity that was not representative of the geometry of the physical specimen. In subsequent work by the same research group [16], the approach was refined, however the simulations were not repeated so we cannot comment on the accuracy of the improved approach.

In the current study a user-defined python script was used to setup the FE models within the ABAQUS CAE pre-processor. The mesh was generated for each ply and further discretised into a number of discrete strips. Cohesive elements representing matrix failure were inserted between adjacent strips to form a contiguous mesh. The distance between cohesive strips (or potential matrix crack paths) was set at 1.0 mm for the 90° plies, which is the validated value in Refs. [13, 14]. For the ±45° plies a structured mesh would prevent a cohesive strip tangential to the edge of the hole, therefore two additional partitions were inserted to further discretise the mesh and allow a strip of cohesive element to be inserted tangential to the edge of the hole. To represent fibre failure the 0° and ±45° plies were further discretised to facilitate insertion of additional cohesive elements to represent fibre failure. The 90° plies are not expected to exhibit fibre failure and therefore do not have cohesive elements inserted to represent fibre failure. The process is repeated for each ply until the full thickness of the laminate has been created. Cohesive elements are inserted between plies of differing orientations allowing the model to represent interlaminar failure. Once the interlaminar cohesive elements have been inserted a contiguous mesh of the entire laminate has been achieved.

The approach used to create the models results in two wedge elements located adjacent to the edge of the hole, as shown in Figure 4. The wedge elements are present in 0°, 90° and ±45° plies. It is reasonable to assume that no continuous fibres span between these two elements as the apex of these elements represents a point of zero thickness. To prevent the build-up of non-physical stresses in these elements a discontinuity is

introduced between these two elements so that the adjacent elements do not share nodes. To demonstrate the importance of this discontinuity, two single ply [0°] samples were analysed. The predicted failure modes for both of these simulations are shown in Figure 5. One sample included the discontinuity between the two wedge elements highlighted in Figure 4 and the other did not. In both models, intralaminar matrix splitting is observed parallel to the fibre, however, when the wedge elements remain connected (Figure 5a) the continuum elements experience in-plane deformation towards the centre of the hole resulting in very high stresses (>3,000MPa) in the connected wedge elements. The stress in the wedge elements far exceeds the fibre rupture strength of IM7/8552. When a discontinuity was introduced between the wedge elements adjacent to the hole edge (Figure 5b) the two halves of the sample are free to translate and the discontinuity prevents these elements from generating non-physical stresses. In order to prevent the build-up of large non-physical stresses in these wedge elements adjacent to the hole edge, a discontinuity was introduced between any wedge elements that were tangential to the edge of the hole.

Please insert figure here.

Figure 4: Detail view of a 0° ply highlighting wedge elements adjacent to the edge of the hole.

Please insert figure here.

Figure 5: Simulated failure modes for a [0°] open hole sample. Symmetry boundary conditions were applied and half the sample simulated. (a) FE model where wedge elements adjacent to the hole remain connected (b) FE model where wedge elements adjacent to the hole are discontinuous.

The current study focusses on failure prediction in quasi-isotropic laminates, therefore the ply angles were limited to 0°, 90°, 45° and -45°. If alternate laminate configurations were analysed such as $[\pm\vartheta]_{ns}$ the resulting FE mesh may have small or skewed elements. The methodology described in the current study is sufficiently robust to handle several elements with poor mesh quality. If the mesh quality for an arbitrary laminate configuration is considered sufficiently poor, this can be corrected by meshing each ply independently and introducing a surface based cohesive contact which is similar to the approach recently proposed in Ref. [31]. One issue associated with a surface based contact is the interaction between matrix cracking and delamination. With an integrated cohesive network the elements are inserted to facilitate interaction between intralaminar matrix cracking and delamination. However, with a surface based contact the displacement jump due to a vertical interlaminar matrix crack may not be transferred to the surface based contact as this will depend on the local master/slave paring. This issue has been described by Van Der Meer and Sluys in their work on the phantom node method and further information is provided in Ref. [13]. The cohesive element based approach described in the present study avoids this issue by inserting cohesive elements at key locations in the model, thereby, allowing interaction between interlaminar matrix cracks and delamination.

The introduction of a surface based contact may increase the overall simulation time compared with an equivalent model employing a cohesive (element) based network. The methodology described herein was intended for use in an implicit FE framework and the cohesive elements used to represent interlaminar failure also prevented

interpenetration of adjacent plies and therefore a penalty based contact was not required. Introducing a surface based cohesive contact, as proposed in Ref. [31], to represent interlaminar failure may increase the overall run-time. If this is an issue then the accuracy of an explicit FE solver could be explored, however, this is outside the scope of the present study.

4 Numerical Predictions and Discussion

This section describes numerical simulations of open hole laminates with FE models enriched with an integrated cohesive network. The simulations demonstrate the suitability of such an approach to simulate progressive damage and ultimate failure in fibre reinforced composite materials. Camanho et al. [29] conducted a series of experiments on open hole samples with varying hole diameters and showed that the ultimate strength was sensitive to the hole size. The differences in strength were due to differing levels of internal damage that correlated with events recorded using acoustic emission.

Camanho et al. [29] successfully predicted the size effect of open hole laminates using a two-dimensional CDM model. The model used a single layer of shell elements and therefore delamination failure was not represented. In their predictions, Camanho et al. [29] did not use the measured ply strengths, rather, the strengths were modified to account for the in-situ effect as described in Ref [32]. The numerical predictions using the measured ply strengths were not reported. Higuchi et al. [25] successfully predicted

the strength of several open hole laminates using an XFEM approach. The XFEM models showed good agreement with experiments using the measured ply strengths that did not account for the in-situ effect. To examine the sensitivity of the predicted open hole strength both the in-situ and measured ply properties were used to predict the size effect of open hole laminates and the predictions compared against experimental data. Subsequently the FE predictions will be designated 'FE_ME' and 'FE_IS' for simulations using the measured and the in-situ ply strengths respectively. A summary of the in-situ and measured material strengths used in the models are provided in Table 3. The in-situ strengths were calculated using the values in Table 1 and Table 2 with the method outlined in Refs. [29, 32]. The non-linear shear correction factor, β, of $2.98X10^{-8}$ was obtained from Ref. [29] and used to calculate the in-situ longitudinal shear strengths. The cohesive zone lengths for mode I and mode II crack propagation were calculated using the approach proposed by Yang and Cox [33]. The maximum in-situ matrix strengths were obtained for an internal ply, see Table 3, with the resulting cohesive zone lengths 0.13mm and 0.24mm for mode I and mode II crack propagation respectively. The critically stressed region is adjacent to the hole and the maximum element size in this region was 0.125mm thereby ensuring a minimum of two integration points within the cohesive zone for mode I crack propagation and at least 4 integration points for mode II crack propagation. For the surface and symmetry plies the in-situ strengths are lower and therefore the cohesive zone lengths are larger and therefore there are more integration points active within the cohesive zone.

Please insert table here.

Table 3: Measured and calculated in-situ strengths (IM7/8552)

It is important to define failure before the results of the simulations are analysed. In the current study, failure is defined as any cohesive element that has a damage index equal to one. A damage index of one corresponds to zero traction across the element, hence a discontinuity in the displacement field. For clarity, any cohesive element with a damage index equal to unity was removed from the visualisation during post-processing. The predicted failure mode for an open hole sample with 2mm diameter hole is shown in Figure 6. The black lines in Figure 6 represent full failed cohesive elements with a damage index equal to unity. These failed cohesive elements represent intralaminar matrix cracking. It should be noted that the model has been separated to allow the internal damage to be visualised. The integrated cohesive network is capable of predicting the ultimate failure of a composite with interlaminar failure, intralaminar matrix splitting and fibre failure explicitly modelled. A continuous path is formed throughout the thickness of the laminate that allows the inception and progression of damage to be simulated.

Please insert figure here.

Figure 6: Ultimate failure of a an IM7/8552 [90/0/±45]3S open hole sample with a hole diameter of 2mm and a W/D of 6. The model used the in-situ ply properties. Note: the model has been separated to facilitate visualisation of the internal damage.

The proposed modelling approach relies on the insertion of cohesive elements along known failure paths. It is therefore important to demonstrate that this approach does not alter the global stiffness of the laminate. Provided that the stiffness of the cohesive elements is greater than the stiffness of the continuum elements the behaviour of the continuum elements should dominate. As a verification the predicted strains at two

locations of an 8mm open hole laminate were compared against experimental results as shown in Figure 7. A strain gauge, SG3, is aligned with the hole center and located 50mm below the centre of the hole. Another, SG2, is aligned with the hole centre and offset 13.5mm. The experimental results were obtained from Camanho et al. [29]. In the initial stages of loading ($0 \leq \sigma \leq 150$MPa), FE models employing both the in-situ and measured ply strengths show good agreement with experimental observations demonstrating that the embedded cohesive network does not influence the global stiffness of the FE model. Upon further loading the model using the measured ply strengths (green curves) under-predicted the strain at location SG2 observed during the experiments. This deviation is due to the initiation and propagation of sub-critical matrix cracking in the outer 90° ply adjacent to the hole. These cracks introduce discontinuities to the outer surface of the ply resulting in a reduction in the local strain. The far field strain, SG3, did not experience any such deviation. In contrast the model using the in-situ ply strengths (orange curves) did not experience this behaviour and the model showed excellent agreement with experimental observations. The predicted evolution of damage for an 8mm open hole model using the in-situ ply strengths is provided in Appendix A. The damage initiates at the edge of the hole in the 90° plies followed by sub-critical matrix cracking in the remaining plies.

Please insert figure here.

Figure 7: Comparison of strain response of an IM7/8552 $[90/0/\pm45]_{3S}$ open hole sample with a hole diameter of 8mm and a W/D of 6. Experimental results (blue) from Camanho et al. [29]. Numerical prediction using the measured ply strengths (green, left) and using the in-situ ply strengths (orange, right)

To further demonstrate that the proposed methodology does not alter the global stiffness of the laminate a comparison of the global strain contours adjacent to the hole were compared to experimental results obtained via DIC. The experiments were reported by Seon [34]. The open hole sample consisted of 16 plies of IM7/8552 with a stacking sequence of $[+45,0,-45,90]_{2S}$. The diameter of the open hole was 6.35mm and the sample had a width to diameter ratio of 6. The DIC contour identifies the evolution of the initial matrix crack in the outer 45 degree ply. A FE model was created for the sample using the approach described previously.

A comparison of the experimental and predicted strain contours are shown in Figure 8 and Figure 9. Qualitatively the FE result shows good agreement with the experimental result. This further validates that the proposed methodology does not alter the global laminate stiffness. It should be noted that the shear strain in both cases is presented in the global Cartesian coordinate system not the local ply coordinate system. This was achieved by transforming the FE strain results from the local (ply) to the global (Cartesian) coordinate system.

Please insert figure here.

Figure 8: Comparison of the global shear strain contours for an IM7/8552 $[+45,0,-45,90]_{2S}$ open hole sample with a hole diameter of 6.35mm and a W/D of 6. Experimental results from Seon [34] and (right) numerical prediction. The top two images were obtained for an applied load of 5080lbf, the bottom two images were obtained for an applied load of 7313lbf.

Please insert figure here.

Figure 9: Comparison of the global normal strain contours for an IM7/8552 $[+45,0,-45,90]_{2S}$ open hole sample with a hole diameter of 6.35mm and a W/D of 6. Experimental results from Seon [34] and (right) numerical prediction. The top two images were obtained for an applied load of 5080lbf, the bottom two images were obtained for an applied load of 7313lbf.

A comparison of the predicted and experimental strengths for several hole diameters is provided in Figure 10. The experimental results are represented in blue and the error bars represent one standard deviation from the mean strength. The established numerical methodology is capable of capturing the size effects over a range of hole diameters. For models using both the measured and in-situ ply strengths the error between the mean experimental strength and the numerical prediction was less than 7.5%.

Please insert figure here.

Figure 10: Comparison of open hole strengths for various hole diameters (W/D=6). Experimental results (blue) from Camanho et al. [29] FE prediction using the measured ply strength (green) and FE prediction using the in-situ ply strengths (orange)

The ability to predict size effects in notched composite structures using a three-dimensional solid model with integrated cohesive elements along potential crack paths has been demonstrated. In-situ and measured ply properties were both capable of predicting the ultimate load in an 8mm open hole sample, however, when the measured ply properties were used more extensive matrix cracking was observed in the outer 90° ply that resulted in a deviation from the experimentally measured strain (see SG2 in Figure 7(left)). When the in-situ ply properties were used the predicted strain showed excellent correlation with the experiment. This is an important finding that is not often

reported. The importance of using the in-situ strength is discussed by Fang et al. and Yang et al. in Refs. [35, 36]. The work reported in Refs. [35, 36] was performed using two-dimensional plane stress elements and the current study has shown that the same sensitivity exists for high fidelity three-dimensional models. One reason for the apparent focus on strength prediction is the difficulty associated with extracting strain information from published DIC images. If the authors do not make the raw DIC data publically available it is difficult to extract the strain history from a published manuscript and therefore analysts often focus on strength prediction. Typically, ultimate static strength prediction is used to assess the accuracy of a numerical modelling approach. Whilst accurate static strength prediction is important, sub-critical matrix cracking can occur well below the ultimate load and these small cracks may propagate when the sample is subjected to fatigue loading. It is important that numerical models are capable of predicting the sub-critical material response and ultimate failure of the sample.

5 Conclusion

The ability to predict damage development and ultimate strength in unidirectional fibre reinforced composite structures using high fidelity Finite Element models has been demonstrated. The modelling approach represented each ply with linear-elastic three-dimensional continuum elements enriched with cohesive interface elements inserted along potential failure paths. A user defined material subroutine was used to represent strength and energy based cohesive failure laws. These elements form a continuous cohesive network, or potential failure path, through the laminate. The cohesive network has the ability to represent matrix cracking and fibre failure discretely and the predicted

damage patterns correlate well with published experimental observations. Future work will focus on expanding the capability of the approach to incorporate a unified failure model capable of simulating damage inception and progression under both static and fatigue loading conditions.

Acknowledgements

This research did not receive any specific grant from funding agencies in the public, commercial, or not-for-profit sectors. The authors would like to express their appreciation to Prof T.E. Tay and Dr M. Ridha from the National University of Singapore for many useful inputs and valuable discussions.

References

[1] Waddoups ME, Eisenmann JR, Kaminski BE. Macroscopic Fracture Mechanics of Advanced Composite Materials. Journal of Composite Materials. 1971;5(4):446-54.
[2] Whitney JM, Nuismer RJ. Stress Fracture Criteria for Laminated Composites Containing Stress Concentrations. Journal of Composite Materials. 1974;8(3):253-65.
[3] Backlund J. Fracture analysis of notched composites. Computers & Structures. 1981;13(1):145-54.
[4] Bažant ZP, Oh BH. Crack band theory for fracture of concrete. Matériaux et Construction. 1983;16(3):155-77.
[5] Su ZC, Tay TE, Ridha M, Chen BY. Progressive damage modeling of open-hole composite laminates under compression. Composite Structures. 2015;122:507-17.
[6] Ridha M, Wang CH, Chen BY, Tay TE. Modelling complex progressive failure in notched composite laminates with varying sizes and stacking sequences. Composites Part A: Applied Science and Manufacturing. 2014;58:16-23.
[7] Ahamed J, Joosten M, Callus P, Wisnom MR, Wang CH. Ply-overlap hybrid technique for joining dissimilar composite materials. Materials & Design. 2016;100(Supplement C):157-67.
[8] Johnson AF, Thomson RS, David M, Joosten MW. 10 - Design and testing of crashworthy aerospace composite components. Polymer Composites in the Aerospace Industry: Woodhead Publishing; 2015. p. 261-93.
[9] Ahamed J, Joosten M, Callus P, John S, Wang CH. Ply-interleaving technique for joining hybrid carbon/glass fibre composite materials. Composites Part A: Applied Science and Manufacturing. 2016;84(Supplement C):134-46.

[10] Iarve EV, Mollenhauer DH. 9 - Mesh-independent matrix cracking and delamination modeling in advanced composite materials A2 - Camanho, Pedro P. In: Hallett SR, editor. Numerical Modelling of Failure in Advanced Composite Materials: Woodhead Publishing; 2015. p. 227-64.
[11] van der Meer FP. Mesolevel Modeling of Failure in Composite Laminates: Constitutive, Kinematic and Algorithmic Aspects. Archives of Computational Methods in Engineering. 2012;19(3):381-425.
[12] Yang QD, Schesser D, Niess M, Wright P, Mavrogordato MN, Sinclair I, et al. On crack initiation in notched, cross-plied polymer matrix composites. Journal of the Mechanics and Physics of Solids. 2015;78:314-32.
[13] van der Meer FP, Sluys LJ. Mesh-independent modeling of both distributed and discrete matrix cracking in interaction with delamination in composites. Engineering Fracture Mechanics. 2010;77(4):719-35.
[14] van der Meer FP, Sluys LJ, Hallett SR, Wisnom MR. Computational modeling of complex failure mechanisms in laminates. Journal of Composite Materials. 2011;46(5):603-23.
[15] Hallett SR, Green BG, Jiang WG, Wisnom MR. An experimental and numerical investigation into the damage mechanisms in notched composites. Composites Part A: Applied Science and Manufacturing. 2009;40(5):613-24.
[16] Achard V, Bouvet C, Castanié B, Chirol C. Discrete ply modelling of open hole tensile tests. Composite Structures. 2014;113:369-81.
[17] Adam L, Bouvet C, Castanié B, Daidié A, Bonhomme E. Discrete ply model of circular pull-through test of fasteners in laminates. Composite Structures. 2012;94(10):3082-91.
[18] Bao H, Liu G. Progressive failure analysis on scaled open-hole tensile composite laminates. Composite Structures. 2016;150:173-80.
[19] Serra J, Bouvet C, Castanié B, Petiot C. Scaling effect in notched composites: The Discrete Ply Model approach. Composite Structures. 2016;148:127-43.
[20] Ataş A, Soutis C. Strength prediction of bolted joints in CFRP composite laminates using cohesive zone elements. Composites Part B: Engineering. 2014;58:25-34.
[21] Hallett SR, Green BG, Jiang W-G, Cheung KH, Wisnom MR. The open hole tensile test: a challenge for virtual testing of composites. International Journal of Fracture. 2009;158(2):169-81.
[22] Cox B, Yang Q. In Quest of Virtual Tests for Structural Composites. Science. 2006;314(5802):1102-7.
[23] Begley MR, Philips NR, Compton BG, Wilbrink DV, Ritchie RO, Utz M. Micromechanical models to guide the development of synthetic 'brick and mortar' composites. Journal of the Mechanics and Physics of Solids. 2012;60(8):1545-60.
[24] Turon A, Camanho PP, Costa J, Dávila CG. A damage model for the simulation of delamination in advanced composites under variable-mode loading. Mechanics of Materials. 2006;38(11):1072-89.
[25] Higuchi R, Okabe T, Nagashima T. Numerical simulation of progressive damage and failure in composite laminates using XFEM/CZM coupled approach. Composites Part A: Applied Science and Manufacturing. 2017;95:197-207.
[26] Tay TE, Sun XS, Tan VBC. Recent efforts toward modeling interactions of matrix cracks and delaminations: an integrated XFEM-CE approach. Advanced Composite Materials. 2014;23(5-6):391-408.

[27] Benzeggagh ML, Kenane M. Measurement of mixed-mode delamination fracture toughness of unidirectional glass/epoxy composites with mixed-mode bending apparatus. Composites Science and Technology. 1996;56(4):439-49.
[28] de Morais AB, Pereira AB. Mixed mode II+III interlaminar fracture of carbon/epoxy laminates. Composites Science and Technology. 2008;68(9):2022-7.
[29] Camanho PP, Maimí P, Dávila CG. Prediction of size effects in notched laminates using continuum damage mechanics. Composites Science and Technology. 2007;67(13):2715-27.
[30] Czabaj MW, Ratcliffe JG. Comparison of intralaminar and interlaminar mode I fracture toughnesses of a unidirectional IM7/8552 carbon/epoxy composite. Composites Science and Technology. 2013;89:15-23.
[31] Falcó O, Ávila RL, Tijs B, Lopes CS. Modelling and simulation methodology for unidirectional composite laminates in a Virtual Test Lab framework. Composite Structures. 2018;190:137-59.
[32] Camanho PP, Dávila CG, Pinho ST, Iannucci L, Robinson P. Prediction of in situ strengths and matrix cracking in composites under transverse tension and in-plane shear. Composites Part A: Applied Science and Manufacturing. 2006;37(2):165-76.
[33] Yang Q, Cox B. Cohesive models for damage evolution in laminated composites. International Journal of Fracture. 2005;133(2):107-37.
[34] Seon G. Finite Element-Based Failure Models for Carbon/Epoxy Tape Composites. : Georgia Institute of Technology; 2009.
[35] Yang QD, Schesser D, Niess M, Wright P, Mavrogordato MN, Sinclair I, et al. On crack initiation in notched, cross-plied polymer matrix composites. Journal of the Mechanics and Physics of Solids. 2015;78(Supplement C):314-32.
[36] Fang XJ, Zhou ZQ, Cox BN, Yang QD. High-fidelity simulations of multiple fracture processes in a laminated composite in tension. Journal of the Mechanics and Physics of Solids. 2011;59(7):1355-73.
[37] Jimenez MA, Miravete A. Application of the Finite-Element Method to Predict the Onset of Delamination Growth. Journal of Composite Materials. 2004;38(15):1309-35.
[38] De Carvalho NV, Chen BY, Pinho ST, Ratcliffe JG, Baiz PM, Tay TE. Modeling delamination migration in cross-ply tape laminates. Composites Part A: Applied Science and Manufacturing. 2015;71:192-203.

Appendix A: Damage progression in an 8mm open hole sample

The evolution of damage for an 8mm IM7/8552 $[90/0/\pm45]_{3S}$ open hole sample is shown in Figure 11. The black lines indicate fully failed cohesive elements (damage index equal to unity). The damage states were taken at various load levels that corresponded to a percentage of the ultimate tensile strength (UTS), shown on the left hand side of the image. A detailed isometric view of the damage progression is shown in addition to the damage state in each ply orientation.

Please insert figure here.

Figure 11: Detail view of damage progression for an IM7/8552 $[90/0/\pm45]_{3S}$ open hole sample with a hole diameter of 8mm and a W/D of 6.

Figures

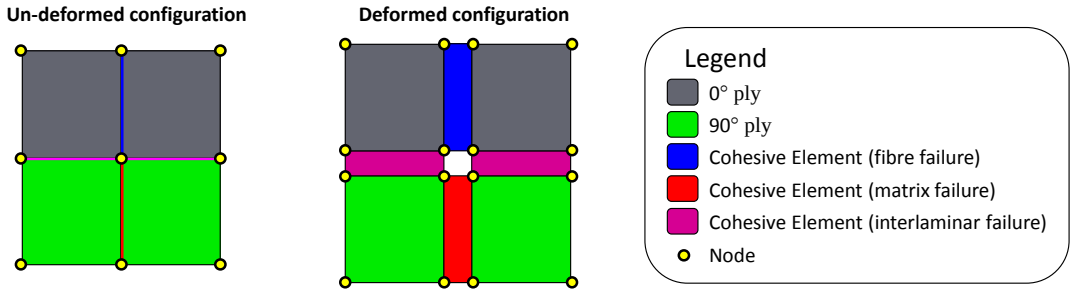

Figure 1: Schematic representation of a brick and mortar modelling approach applied to a unidirectional fibre reinforced composite. Note: the deformed configuration shows an exaggerated displacement.

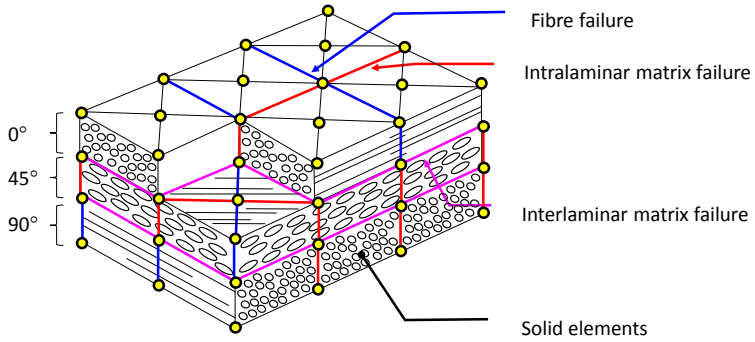

Figure 2: Representation of a [0,45,90] laminate modelled with an integrated cohesive network. The filled yellow circles represent nodes and the bold blue, red and magenta lines represent cohesive elements inserted to represent fibre failure, intralaminar matrix failure and interlaminar matrix failure respectively. Note: The lower corner of the 0° ply has been removed to facilitate visualisation of the cohesive network.

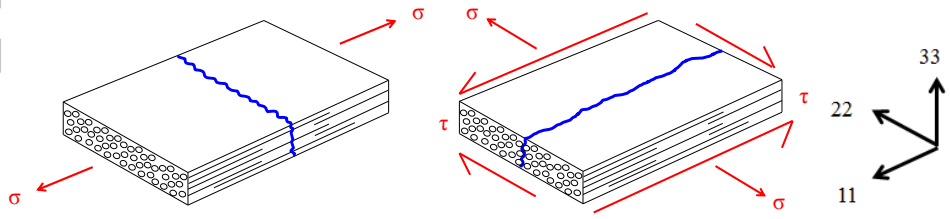

Figure 3: Intralaminar failure modes (left) fibre failure (right) matrix failure.

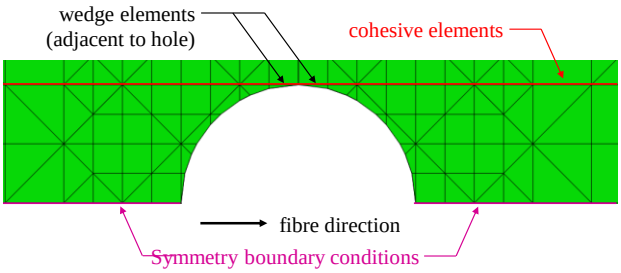

Figure 4: Detail view of a 0° ply highlighting wedge elements adjacent to the edge of the hole.

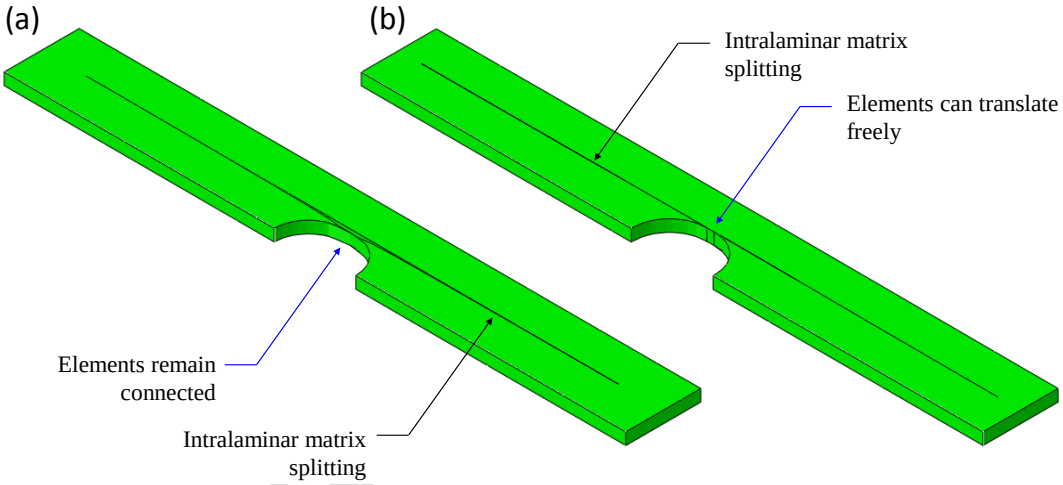

Figure 5: Simulated failure modes for a [0°] open hole sample. Symmetry boundary conditions were applied and half the sample simulated. (a) FE model where wedge elements adjacent to the hole remain connected (b) FE model where wedge elements adjacent to the hole are discontinuous.

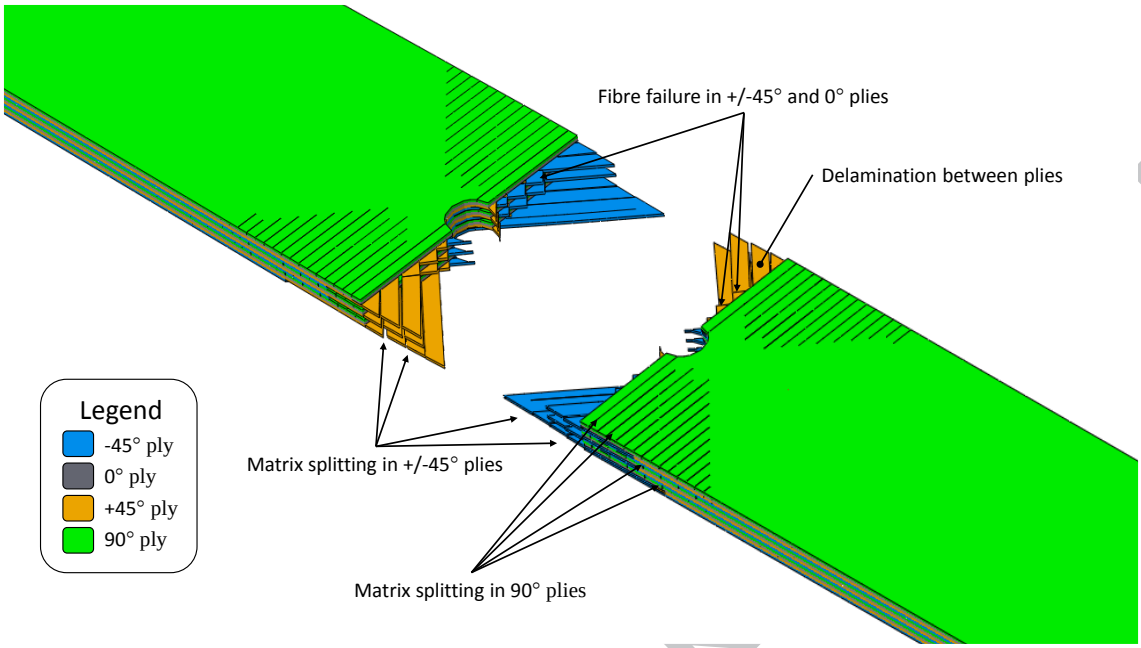

Figure 6: Ultimate failure of a an IM7/8552 [90/0/±45]3S open hole sample with a hole diameter of 2mm and a W/D of 6. The model used the in-situ ply properties. Note: the model has been separated to facilitate visualisation of the internal damage.

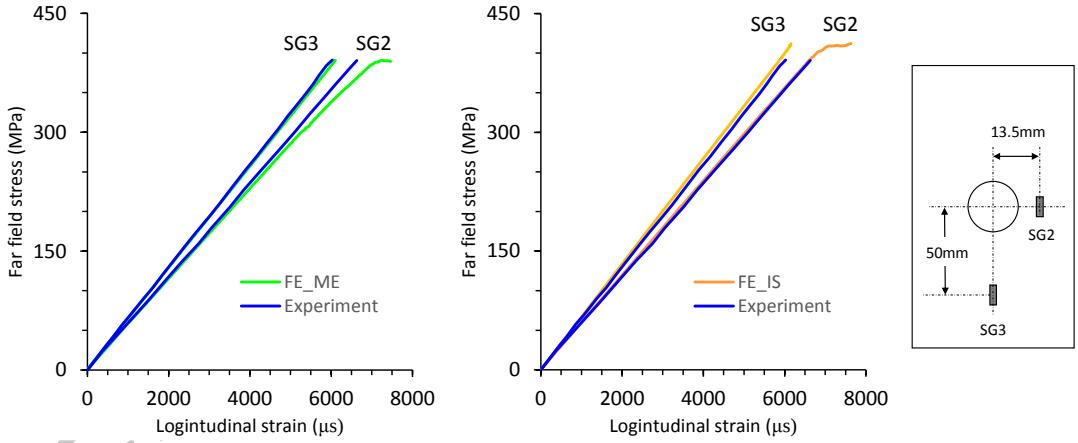

Figure 7: Comparison of strain response of an IM7/8552 [90/0/±45]3S open hole sample with a hole diameter of 8mm and a W/D of 6. Experimental results (blue) from Camanho et al. [29]. Numerical prediction using the measured ply strengths (green, left) and using the in-situ ply strengths (orange, right)

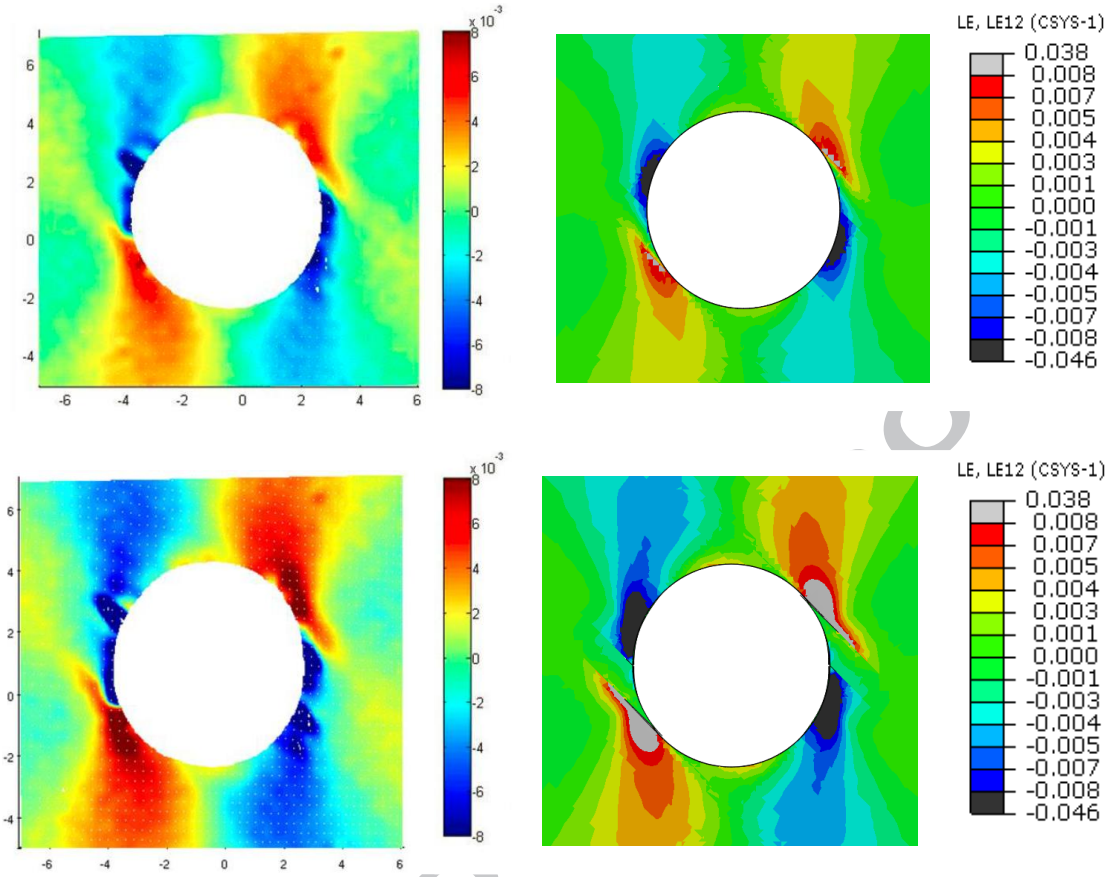

Figure 8: Comparison of the global shear strain contours for an IM7/8552 $[+45,0,-45,90]_{2S}$ open hole sample with a hole diameter of 6.35mm and a W/D of 6. Experimental results from Seon [34] and (right) numerical prediction. The top two images were obtained for an applied load of 5080lbf, the bottom two images were obtained for an applied load of 7313lbf.

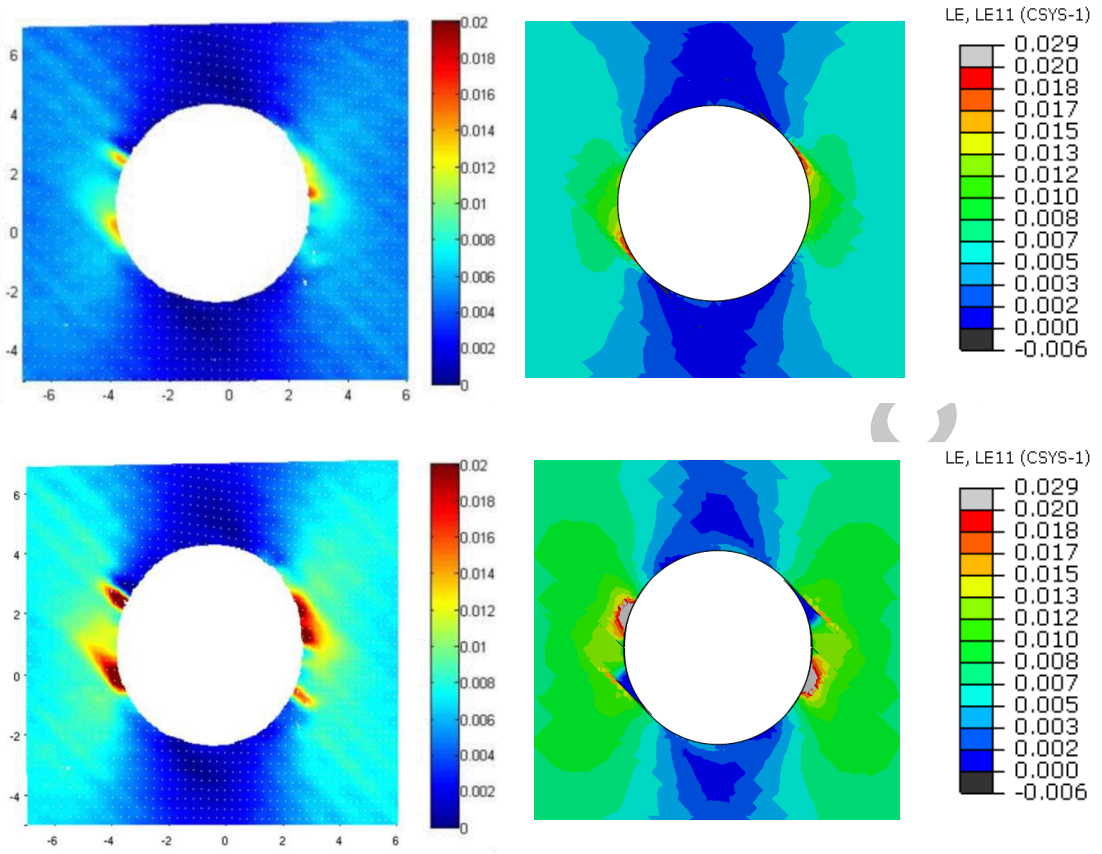

Figure 9: Comparison of the global normal strain contours for an IM7/8552 $[+45,0,-45,90]_{2S}$ open hole sample with a hole diameter of 6.35mm and a W/D of 6. Experimental results from Seon [34] and (right) numerical prediction. The top two images were obtained for an applied load of 5080lbf, the bottom two images were obtained for an applied load of 7313lbf.

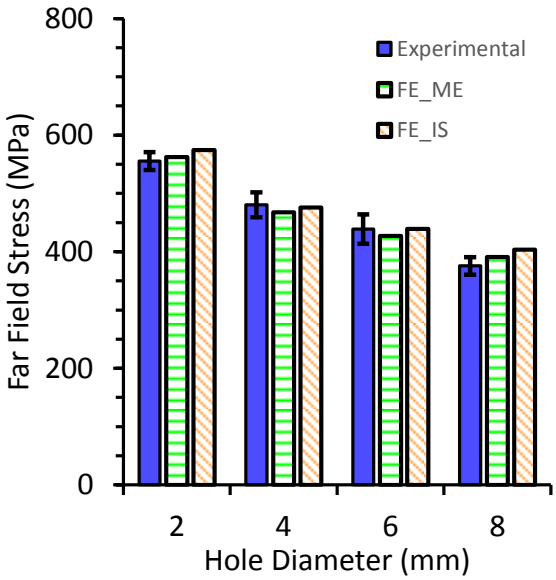

Figure 10: Comparison of open hole strengths for various hole diameters (W/D=6). Experimental results (blue) from Camanho et al. [29] FE prediction using the measured ply strength (green) and FE prediction using the in-situ ply strengths (orange)

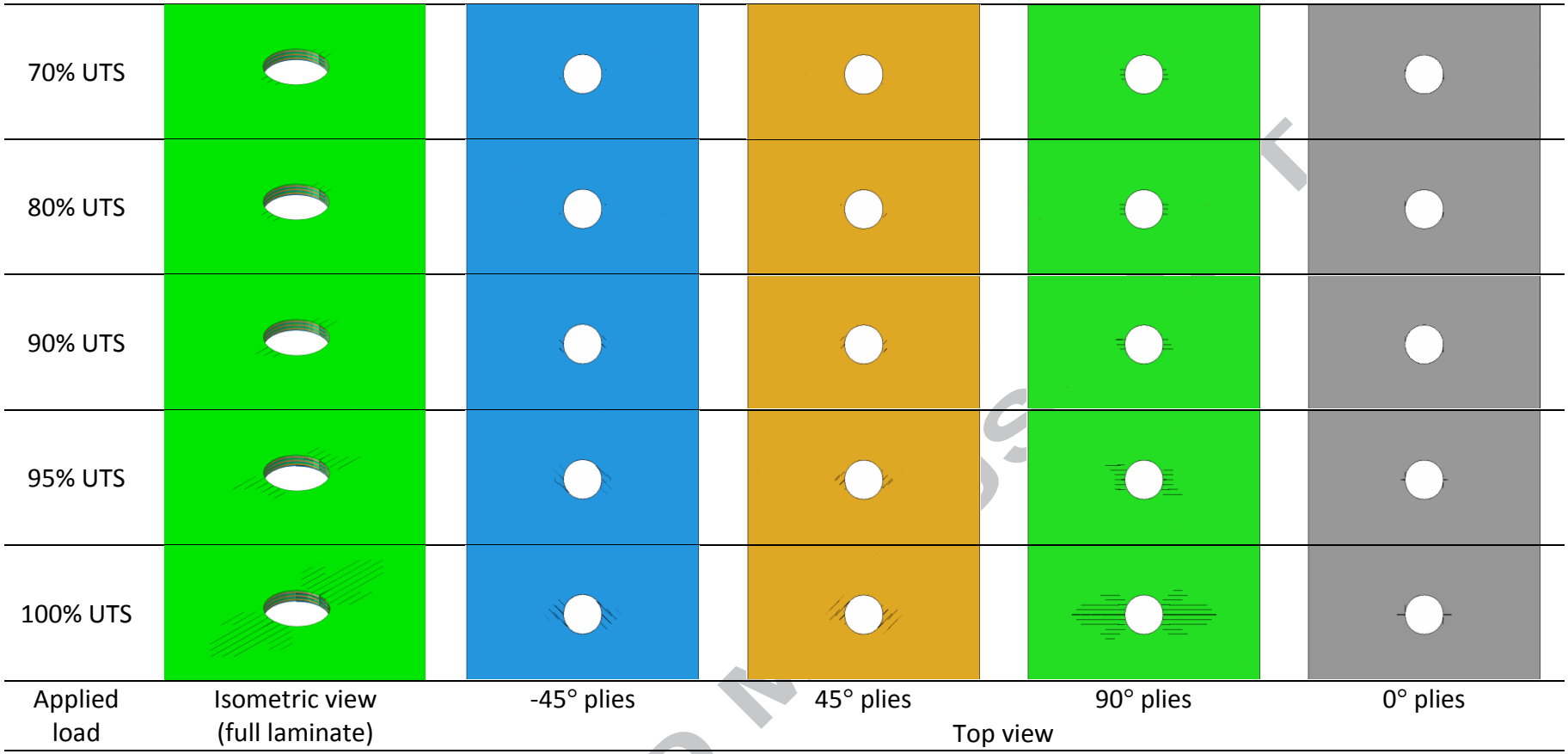

Figure 11: Detail view of damage progression for an IM7/8552 [90/0/±45]3S open hole sample with a hole diameter of 8mm and a W/D of 6.

Tables

Table 1: Orthotropic Material Properties for IM7/8552

Description	Symbol	Value	Units	Reference
Longitudinal modulus	E_{11}	160,580	MPa	[37]
Transverse Modulus	$E_{22} = E_{33}$	11,500	MPa	[37]
Longitudinal Poisson's ratio	$\upsilon_{12} = \upsilon_{13}$	0.31	-	[37]
Transverse Poisson's ratio	υ_{23}	0.49	-	[37]
Longitudinal shear modulus	$G_{12} = G_{13}$	5,430	MPa	[37]
Transverse shear modulus	G_{23}	3,840	MPa	[37]
Longitudinal thermal expansion coefficient	α_{11}	-5.5×10^{-6}	Strain/°C	[29]
Transverse thermal expansion coefficient	$\alpha_{22} = \alpha_{33}$	25.8×10^{-6}	Strain/°C	[29]
Ply thickness	t_{ply}	0.131	mm	[29]

Table 2: Strength and Fracture Energies Associated with Fibre Rupture and Matrix Cracking (IM7/8552)

Description	Symbol	Value	Units	Reference
Fibre failure parameters				
Fibre rupture strength	S_{11}	2,326.2	MPa	[29]
Fracture energy associated with fibre rupture	G_{FT}	81.5	kJ/m^2	[29]
Matrix failure parameters				
Transverse tensile strength	$S_{22} = S_{33}$	62.3	MPa	[29]
Longitudinal shear strength	$S_{12} = S_{13}$	92.3	MPa	[29]
Transverse shear strength	S_{23}	75.3	MPa	[29]
Mode I fracture energy	G_I	0.21	kJ/m^2	[38]
Mode II fracture energy	G_{II}	0.77	kJ/m^2	[38]
Interaction parameter (BK)	η	2.1	-	[38]

Table 3: Measured and calculated in-situ strengths (IM7/8552)

Description	Symbol	Measured Value	In-situ values			Units
			External ply	Internal ply	Symmetry ply	
Transverse tensile strength	$S_{22} = S_{33}$	62.3	98.5	156.6	110.7	MPa
Longitudinal shear strength	$S_{12} = S_{13}$	92.3	109.6	131.7	90.7	MPa